# Increase in the conformational flexibility of $\beta_2$-microglobulin upon copper binding: A possible role for copper in dialysis-related amyloidosis

JAMES VILLANUEVA,[1,4,5] MASARU HOSHINO,[1,4] HIDENORI KATOU,[1]
JÓZSEF KARDOS,[1] KAZUHIRO HASEGAWA,[2] HIRONOBU NAIKI,[2,3] AND YUJI GOTO[1,3]

[1]Institute for Protein Research, Osaka University, Yamadaoka 3-2, Suita, Osaka 565-0871, Japan
[2]Department of Pathology, Fukui Medical University, Matsuoka, Fukui 910-1193, Japan
[3]CREST, Japan Science and Technology Agency, Kawaguchi, Saitama 332-0012, Japan

(RECEIVED September 19, 2003; FINAL REVISION October 24, 2003; ACCEPTED November 10, 2003)

**Abstract**

A key pathological event in dialysis-related amyloidosis is the fibril formation of $\beta_2$-microglobulin (β2-m). Because β2-m does not form fibrils in vitro, except under acidic conditions, predisposing factors that may drive fibril formation at physiological pH have been the focus of much attention. One factor that may be implicated is $Cu^{2+}$ binding, which destabilizes the native state of β2-m and thus stabilizes the amyloid precursor. To address the $Cu^{2+}$-induced destabilization of β2-m at the atomic level, we studied changes in the conformational dynamics of β2-m upon $Cu^{2+}$ binding. Titration of β2-m with $Cu^{2+}$ monitored by heteronuclear NMR showed that three out of four histidines (His13, His31, and His51) are involved in the binding at pH 7.0. $^{1}H$-$^{15}N$ heteronuclear NOE suggested increased backbone dynamics for the residues Val49 to Ser55, implying that the $Cu^{2+}$ binding at His51 increased the local dynamics of β-strand D. Hydrogen/deuterium exchange of amide protons showed increased flexibility of the core residues upon $Cu^{2+}$ binding. Taken together, it is likely that $Cu^{2+}$ binding increases the pico- to nanosecond fluctuation of the β-strand D on which His51 exists, which is propagated to the core of the molecule, thus promoting the global and slow fluctuations. This may contribute to the overall destabilization of the molecule, increasing the equilibrium population of the amyloidogenic intermediate.

**Keywords:** Amyloid fibrils; copper binding; dialysis-related amyloidosis; heteronuclear NMR; hydrogen/deuterium exchange; $\beta_2$-microglobulin; protein folding/misfolding

**Supplemental material:** See www.proteinscience.org

A growing number of proteins having the propensity to misfold and form amyloid fibrils have been recognized to be associated with the pathology of some important human diseases (Kelly 1998; Rochet and Lansbury Jr. 2000). These fibrils are characterized by a cross-β structure where β-strands are perpendicularly oriented to the axis of the polymeric fibril (Sunde et al. 1997; López et al. 2002). One such disease is dialysis-related amyloidosis, a debilitating complication acquired by patients undergoing long-term hemodialysis characterized by the deposition of $\beta_2$-microglobulin (β2-m) amyloid fibrils in the synovial tissue, joint cartilage, and bone tissue (Gejyo et al. 1985; Geyjo and Arakawa 1990). β2-m is the light chain constituent of the class I major histocompatibility (MHC) complex (Bjorkman et al. 1987). It is a 12-kD protein composed of 99 amino acids that forms a typical immunoglobulin domain fold, that is, seven β-strands arranged in a β-sandwich and stabilized

Reprint requests to: Yuji Goto, Institute for Protein Research, Osaka University, Yamadaoka 3-2, Suita, Osaka 565-0871, Japan; e-mail: ygoto@protein.osaka-u.ac.jp; fax: 081-6-6879-8616.

[4]These authors contributed equally to this work.

[5]Present address: Institute of Chemistry, University of the Philippines, Diliman, Quezon City, Philippines.

*Abbreviations:* β2-m, $\beta_2$-microglobulin; CD, circular dichroism; H/D, hydrogen/deuterium; HSQC, heteronuclear single quantum coherence; NMR, nuclear magnetic resonance; NOE, η, nuclear Overhauser effect; $R_1$, longitudinal relaxation rates; TOCSY, total correlation spectroscopy.

Article published online ahead of print. Article and publication date are at http://www.proteinscience.org/cgi/doi/10.1110/ps.03445704.

by hydrophobic interactions as well as a single disulfide bond between Cys25 and Cys80 (Bjorkman et al. 1987; Trinh et al. 2002; Verdone et al. 2002).

The formation of β2-m amyloid fibrils in vivo and in vitro has been extensively studied (Naiki et al. 1997; McParland et al. 2000; Chiti et al. 2001a,b; Heegaard et al. 2001; Kad et al. 2001, 2003). We analyzed the amyloid fibrils prepared by the seed-dependent extension reaction by using a novel procedure that combines hydrogen/deuterium (H/D) exchange of amide protons, dissolution of exchanged fibrils by dimethylsulfoxide, and 2D NMR analysis (Hoshino et al. 2002). It is noted that a similar procedure was independently developed by others, and was applied to the model amyloid fibrils formed by cold shock protein A (Alexandrescu 2001) or amyloidogenic fragment of Alzheimer β-peptide (Ippel et al. 2002). Our results with β2-m amyloid fibrils indicated that most of the residues in the middle region of the molecule, including the loop regions in the native structure, form a β-sheet core, explaining the marked rigidity of amyloid fibrils (Hoshino et al. 2002).

Several studies have offered some hints as to how these fibrils are formed from β2-m in the native state. A partially unfolded conformation of β2-m, having a higher propensity to aggregate compared to the native state in an environment close to physiological conditions, has been isolated using capillary electrophoresis (Chiti et al. 2001a; Heegaard et al. 2001). β2-m, lacking six residues in the N terminus, has been shown to increase amyloidogenicity, and has been found ex vivo together with other truncated species (Esposito et al. 2000). McParland et al. (2002) reported that an amyloid precursor that accumulated at pH 3.6 retains a stable structure in five (B, C, D, E, and F) of the seven β-strands that comprise the hydrophobic core of the native protein. They suggested that this stable region is important for amyloid fibril formation. Because the optimal pH for amyloid fibril formation by the seed-dependent extension reaction is 2.5, where the protein is more unfolded, we proposed that the more disordered structure is important for amyloid fibril formation (Katou et al. 2002). We identified the minimal peptide fragment (residues 20–41) responsible for the amyloidogenic property of β2-m, which is substantially unfolded by itself (Kozhukh et al. 2002). Recently, we showed that an 11-residue peptide, Gln21-H31, also forms amyloid fibrils (Hasegawa et al. 2003). On the other hand, Jones et al. (2003) have identified that another peptide, Asp59–Thr71, form amyloid fibrils. More recently, studying the kinetics of spontaneous assembly of amyloid fibrils of β2-m at pH 2.5, Kad et al. (2003) suggested that various kinds of protein aggregates may act as nucleation sites.

One of the factors that could play a significant role in triggering β2-m amyloid fibril formation in vivo is interaction with transition metals, particularly $Cu^{2+}$. As described by Morgan et al. (2001), although the majority of $Cu^{2+}$ is tightly bound to plasma proteins, the dialysis procedure has two potential ways of allowing interaction of β2-m with free $Cu^{2+}$: one is with $Cu^{2+}$ in dialysate, and the other is with $Cu^{2+}$ in cellulose membranes. Using urea and thermal denaturation as assessed by changes in intrinsic fluorescence, Morgan et al. (2001) have proven that the native β2-m is destabilized in the presence of $Cu^{2+}$ at pH 7.4. They estimated a dissociation constant of 2.7 μM assuming an equimolar stoichiometry of $Cu^{2+}$ for β2-m. $Cu^{2+}$ binding has been shown to be specific compared with the nonspecific binding of $Ca^{2+}$ and $Zn^{2+}$ with β2-m. Eakin et al. (2002) further examined the effect of several divalent metal ions on the stability of β2-m, showing that β2-m is specifically destabilized by $Cu^{2+}$. Out of the four histidine residues in β2-m (His13, His31, His51 and His84), Verdone et al. (2002) identified His31 and His13 as $Cu^{2+}$ binding sites by performing $Cu^{2+}$ titrations of β2-m using $^{1}H$ -2D TOCSY at pH 6.6. They suggested that $Cu^{2+}$ binding may easily perturb the hydrophilic/hydrophobic balance, leading to the formation of a partially unfolded intermediate. With mutagenesis of potential coordinating histidine residues for $Cu^{2+}$, Eakin et al. (2002) reported that, although β2-m binds $Cu^{2+}$ specifically at His31 in the native state at pH 7.0–7.4, the binding of $Cu^{2+}$ by nonnative states of β2-m at His13, His51, and His84 is responsible for overall destabilization.

The medical implications of the involvement of $Cu^{2+}$ in β2-m amyloidosis are important because about 30% of the commercially available ultrafiltration membranes used in dialysis therapy contain $Cu^{2+}$, which could easily leak out to the plasma, thus promoting fibril formation (Morgan et al. 2001). In a wider context, $Cu^{2+}$ and other transition metals have also been associated with other amyloidogenic proteins. $Zn^{2+}$ and $Cu^{2+}$ in particular have been shown to strongly induce Aβ aggregation in a pH-dependent manner (Atwood et al. 1998; Liu et al. 1999; Miura et al. 2000). Numerous studies have also been done on the binding of $Cu^{2+}$ with prion protein (Stockel et al. 1998; Kramer et al. 2001). Synthetic peptides corresponding to the octapeptide repeat region of prion protein have been shown to bind $Cu^{2+}$ with three sites available at pH 6.0 and four to five $Cu^{2+}$-binding sites at pH 7.4. $Cu^{2+}$ has also been associated with fibril formation of the pathogenic immunoglobulin light chain (Davis et al. 2001).

In this study, using heteronuclear NMR techniques, we have probed changes in the conformational dynamics of β2-m upon $Cu^{2+}$ binding that may provide insight into its role in dialysis-related amyloidosis. First, to verify that $Cu^{2+}$ destabilizes the native state, thermal denaturation using CD was performed. Effects of $Cu^{2+}$ on the conformational dynamics of the β2-m structure were followed using $^{1}H$-$^{15}N$ 2D NMR to identify perturbed sites. Steady-state $\{^{1}H\}$-$^{15}N$ heteronuclear NOE was used to monitor restricted backbone motions in the pico- to nanosecond time scale after considering the paramagnetic contribution of $Cu^{2+}$ ion. Backbone amide H/D exchange was carried out to examine the effects of $Cu^{2+}$ on the flexibility of the core residues.

## Results

### *Thermal denaturation*

The heat stability of the native β2-m is nearly constant in the pH range of 6.2–8.0, as judged by thermal denaturation experiments followed by CD (Fig. 1, $\Delta G_U$~23–24 kJ/mole at 25°C). The protein and metal concentrations for the study of the effect of $Cu^{2+}$ on the stability of β2-m were chosen to get a similar extent of saturation of $Cu^{2+}$ as in the NMR measurements: 5 μM β2-m and 50 μM $Cu^{2+}$ for the CD measurements versus 0.5 mM β2-m and 0.5 mM $Cu^{2+}$ for the NMR measurements, resulting a saturation of ~0.94 for both measurements, estimated from a dissociation constant of 2.7 μM of $Cu^{2+}$ on β2-m (Morgan et al. 2001). Destabilization of β2-m in the presence of $Cu^{2+}$ at pH 7.0 was evident from the denaturation curves monitored by ellipticity at 220 nm (Fig. 1, lines 1,3), confirming previous results using tryptophan fluorescence (Morgan et al. 2001; Eakin et al. 2002). Although the validity of a two-state transition is ambiguous, especially in the presence of $Cu^{2+}$, it will be useful to compare quantitatively the effects of $Cu^{2+}$ on the stability of β2-m. The curve-fitting assuming a two-state transition indicated that $T_m$ in the presence of $Cu^{2+}$ is 55.4°C as opposed to 63.0°C in the absence of $Cu^{2+}$, showing a difference of 7°C. $\Delta G_U$ values in the absence and presence of $Cu^{2+}$ at 25°C were estimated to be 23.3 kJ/mole and 13.4 kJ/mole, respectively. A previous study (Morgan et al. 2001) reported the $\Delta G_U$ values in the absence and presence of 100 μM $Cu^{2+}$ at pH 7.4 and 25°C to be 27.9 kJ/mole and 9.4 kJ/mole, respectively. For comparison, $\Delta G_U$ at pH 8.5 and 5°C was estimated to be 34 kJ/mole from the unfolding transition induced by guanidine hydrochloride (Ohhashi et al. 2002).

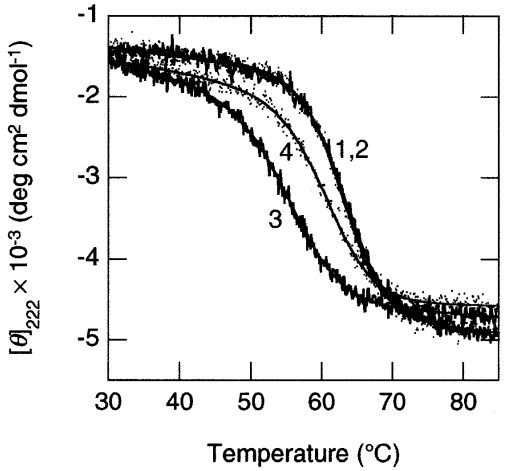


**Figure 1.** Thermal denaturation of β2-m followed by ellipticity at 220 nm in the absence of $Cu^{2+}$ at pH 7.0 (solid line, *1*) and pH 6.5 (dots, *2*) and in the presence of $Cu^{2+}$ at pH 7.0 (solid line, *3*) and pH 6.5 (dots, *4*). Note that in the absence of $Cu^{2+}$, the two transition curves obtained at pH 7.0 and pH 6.5 are overlapping. The protein and $Cu^{2+}$ concentrations were 5 μM and 50 μM $CuCl_2$, respectively, where the $Cu^{2+}$ concentration is high enough to form the complex (Morgan et al. 2001). The fitted theoretical lines on the basis of standard thermodynamic equations (Nishii et al. 1995) are also plotted. In the curve fittings, $\Delta C_{p,U}$ was assumed to be 5.6 kJ/mole/K. In the absence of $Cu^{2+}$, $T_m$, $\Delta H_m$ and $\Delta G_U$(25°C) were 63.0°C, 317 kJ/mole and 23.3 kJ/mole, respectively, at pH 7.0, and 62.8°C, 319 kJ/mole and 23.5 kJ/mole, respectively, at pH 6.5. In the presence of $Cu^{2+}$, the values were 55.4°C, 232 kJ/mole and 13.4 kJ/mole, respectively, at pH 7.0, and 60.7°C, 271 kJ/mole and 17.9 kJ/mole, respectively, at pH 6.5.

Interestingly, at pH 6.5 (Fig. 1, dots 2,4), the extent of destabilization by $Cu^{2+}$ was less. The midpoint temperature of the transition in the absence of $Cu^{2+}$ was 62.8°C, showing a virtually identical value to that at pH 7.0, while in the presence of $Cu^{2+}$, the $T_m$ value decreased only slightly to 60.7°C. $\Delta G_U$ values in the absence and presence of $Cu^{2+}$ at 25°C were estimated to be 23.5 kJ/mole and 17.9 kJ/mole, respectively. These results clearly demonstrated that the affinity of $Cu^{2+}$ for β2-m was weaker at pH 6.5 than at pH 7.0, in good agreement with titration experiments (see below).

### *Copper binding sites*

Assignments for the backbone peak resonances have been reported previously (Katou et al. 2002), where 95 of 97 expected residues have been unambiguously assigned (Fig. 2A). In the presence of 0.17 mM $Cu^{2+}$ at 0.37 mM β2-m, peak intensities of many residues decreased, whereas others remained the same without a notable change in the chemical shift values (Fig. 2B). Although only a small proportion of the molecules were complexed with $Cu^{2+}$, the fast-exchange averaging of the paramagnetic metal ion probably produced notable perturbations. Line broadening and a loss of peak intensity could be observed for residues close to $Cu^{2+}$ due to its large electron relaxation rate, the effect of which diminishes according to the inverse-sixth power of the interatomic distance.

Site-specific perturbations caused by $Cu^{2+}$ binding at pH 6.5 and pH 7.0 were examined by plotting the peak intensities against the residue number (Fig. 3). The effects were not clear at a very low $Cu^{2+}$ concentration of 0.1 μM at pH 6.5. By increasing the $Cu^{2+}$ concentration to 0.8 mM, it became clear that the residues close to His13 and His31 were significantly affected (Fig. 3B). Under the same conditions, His51 and His84 were less affected. On the other hand, at pH 7.0, all of His13, His31, and His51 were clearly affected by the presence of 0.8 mM $Cu^{2+}$ (Fig. 3C,D). Again, His84 was less affected than others. At both pH 6.5 and 7.0, the N-terminal regions including β-strand A were notably affected by the presence of 0.8 mM $Cu^{2+}$. The specific binding of $Cu^{2+}$ ion to these three histidine residues were also indicated by significant increase in the longitudinal relaxation rate, $R_1$, in the presence of $CuCl_2$ at pH 7.0 (see below).

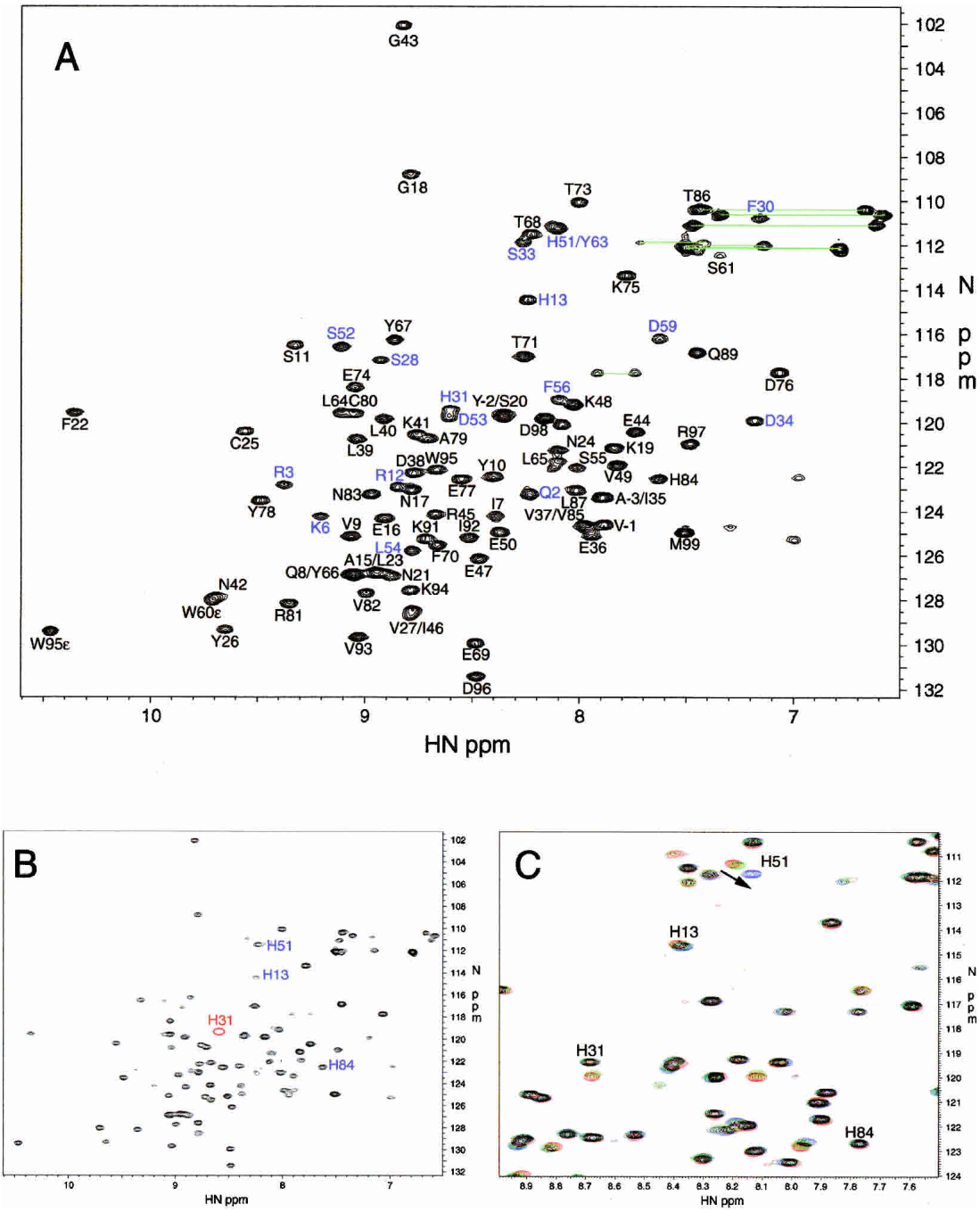


**Figure 2.** (*A*) $^{1}$H-$^{15}$N HSQC spectra of β2-m at pH 7.0 and 25°C. Protein concentration was 0.37 mM. The backbone assignments are indicated by amino acid name and residue number. The blue labels indicate the residues notably affected by the addition of $Cu^{2+}$. Green lines indicate the pairs of resonances from Gln/Asn side chain. (*B*) $^{1}$H-$^{15}$N HSQC spectra of β2-m in the presence of $Cu^{2+}$ at pH 7.0 and 25°C. Protein and $Cu^{2+}$ concentrations were 0.37 mM and 0.17 mM, respectively. The four histidine residues are indicated. The completely disappeared histidine (His31) are indicated by red label and circle. (*C*) Overlay of the NMR spectra at pH 6.2 (red), pH 6.5 (green), and pH 7.0 (blue), showing the pH-dependent shift of the His51 peak. The four histidine peaks are labeled accordingly. These spectra were recorded at 37°C.

Our results at pH 6.5 are consistent with those of Verdone et al. (2002) at pH 6.5 implying that only His13 and His31 are involved in $Cu^{2+}$ binding. On the other hand, the results at pH 7.0 showed that His51 is also involved in the interaction with $Cu^{2+}$. Consistent with this, the decrease in stability of β2-m in the presence of $Cu^{2+}$ at pH 6.5 was less

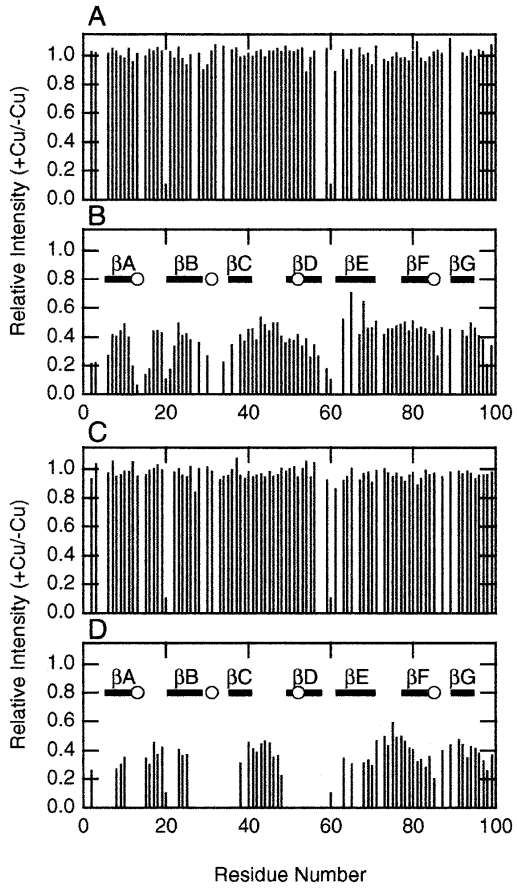


**Figure 3.** Ratios of peak intensities of $^1$H-$^{15}$N HSQC spectra in the presence and absence of $Cu^{2+}$ at pH 6.5 (*A*,*B*) and at pH 7.0 (*C*,*D*). Higher ratios (*A*,*C*) indicate less effect on the residues, while low values indicate larger perturbations (*B*,*D*). The following 16 residues were not used because of the absence of amide protein or low resolution of the peaks: I1, T4, P5, P14, S20, V27, P32, I35, K58, W60, F62, Y66, P72, S88, P90, and K91. The protein concentration was 0.33 mM and $Cu^{2+}$ concentration was 0.1 μM for *A* and *C* and 0.8 mM for *B* and *D*. Titration was done at 25°C. In *B* and *D*, the locations of secondary structures obtained from the X-ray structure (*7*) and His residues are indicated.

than that at pH 7.0 (Fig. 1). In contrast, Eakin et al. (2002) reported that the interactions of His13 with $Cu^{2+}$ are dominant in the native state at pH 7.0–7.4. The involvement of three histidines at pH 7.0 instead of two at pH 6.5 may be due to a difference in the protonation state of His51. To address the difference in protonation states at pH 6.5 and pH 7.0, we measured the $^1$H-$^{15}$N HSQC spectrum at pH 6.2, pH 6.5, and pH 7.0 (Fig. 2C). Among many peaks, a pH-dependent peak shift was observed only for His51. This indicates that deprotonation of His51, enabling $Cu^{2+}$ binding, indeed occurs between pH 6.5 and pH 7.0. A link between the deprotonation of histidines and $Cu^{2+}$ binding was also proposed for the Alzheimer β-amyloid and the prion protein (Atwood et al. 1998; Stockel et al. 1998).

The residues significantly affected by the addition of $Cu^{2+}$ at pH 7.0 are indicated in the 3D structure of β2-m, where the locations of four histidine residues are also given (Fig. 4A). It can be seen that most of the affected residues are located near to the $Cu^{2+}$ binding sites, for instance, His13, His31, and His51.

### *Backbone dynamics*

The steady-state {$^1$H}-$^{15}$N NOE values can be used as a gauge in describing pico- to nanosecond time scale backbone dynamics that reflect internal motions in the protein (Viles et al. 2001). {$^1$H}-$^{15}$N NOE values were calculated in the absence and presence of $Cu^{2+}$ at pH 7.0 and 25°C (Fig. 5B). For β2-m without $Cu^{2+}$, decreased NOE values were observed at the N and C termini as well as in the loop regions (Ile46, Glu47, Lys48, Val49, Glu50, and Lys75), which are typical of a globular protein (Hoshino et al. 2000; Werner et al. 2000; Tollinger et al. 2001). On the other hand, the complex of β2-m with $Cu^{2+}$ showed a further decrease in the NOE value for several residues. Intriguingly, most of the affected residues are located near to His51 (Fig. 5B).

Although the steady-state {$^1$H}-$^{15}$N NOE is known to highly depend on the internal dynamic motions on pico- to nanosecond time scale, the direct comparison of the values in the absence and presence of $Cu^{2+}$ is difficult, because the binding of $Cu^{2+}$ ions affects the NOE values through the increase in $R_1$. To eliminate the paramagnetic contributions and extract the net effect of $Cu^{2+}$ binding on the protein's dynamic motions, we introduced a new representation, the product of $R_1$ and NOE, which becomes independent of the paramagnetic effect (Fig. 5C; see Discussion). The corrected NOE for Asp49 and Ser55 still showed significant decrease upon the addition of $Cu^{2+}$ ion. Because we could not obtain $R_1$ for other residues on β-strand D, their corrected NOE values are unknown. Nevertheless, the results suggest the increased pico- to nanosecond time scale dynamics of the residues near His51, probably most residues on β-strand D. The increased dynamics was also suggested for the N-terminal residues, while the C-terminal residues showed no significant change.

### *Amide H/D exchange*

To address the effect of $Cu^{2+}$ on the protected elements of the secondary structure, H/D exchange experiments were done at 25°C and a $pD_r$ of 7.0. After 40 min of exchange in the absence of $Cu^{2+}$, only 28 residues out of 95 were visible in the $^{15}$N-$^1$H HSQC spectrum, showing that not many residues are highly protected from exchange (Fig. 6A). After 22 h, several highly protected residues were still clearly seen (Fig. 6B). For each of the 28 protected residues, kinetics of H/D exchange were represented by plotting peak intensities against time (Fig. 7). The kinetics were fitted to a single exponential curve to obtain the apparent exchange rate

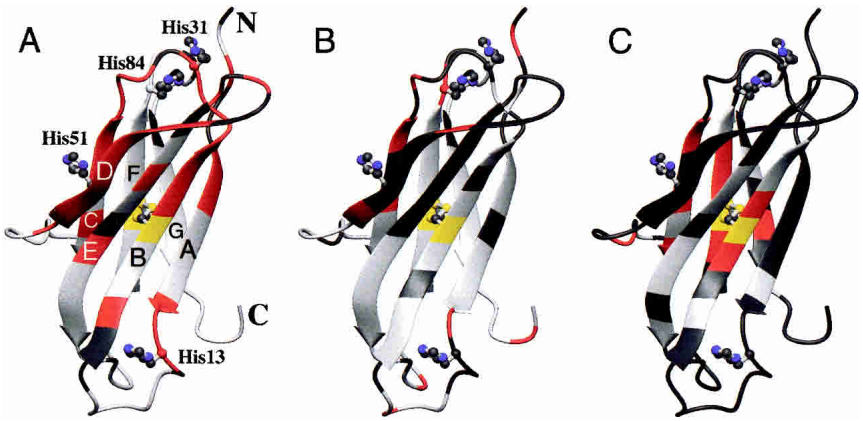


**Figure 4.** Structures of β2-m showing residues perturbed upon $Cu^{2+}$ binding. (*A*) The residues that showed a significant decrease in intensity in the presence of $Cu^{2+}$. The residues observed in the absence of $Cu^{2+}$ but disappeared in Figure 3D are labeled in red. Other residues present in Figure 3D are labeled in white. (*B*) The residues with the decreased value of $\eta \times R_1$ in the presence of $Cu^{2+}$. The residues with the decrease larger than 0.1 in Figure 5C are labeled in red, and those with the decrease less than 0.1 are labeled in white. (*C*) The residues with an increased H/D exchange rate in the presence of $Cu^{2+}$. The residues with the ratio higher than 1.5 are labeled in red, and those with the ratio less than 1.5 are labeled in white. The residues not used for the analysis are labeled in gray, and the two cysteine residues (Cys25 and Cys80) are labeled in yellow. The side chains of histidine residues are indicated. The 3D structures were drawn by MOLMOL (Koradi et al. 1996).

($k_{app}$). Exchange rates for residues His84, Thr86, and Asp98 were not determined as these residues disappeared quickly in the time course of the experiment. Residues with signal overlap such as Gln8, Ala15, Leu23, His51, Tyr63, and Tyr66 were also precluded from the analysis. The protection factor ($P$) was defined by $k_{int}/k_{ex} = P$, where $k_{int}$ is the exchange rate in the random coil conformation (Bai et al. 1993; Connelly et al. 1993). The $P$ values determined for all the residues available (Supplemental Material: Table 1) are plotted against the residue number (Fig. 5D).

For β2-m without $Cu^{2+}$, $P$ values of the protected residues varied from $10^4$ to $10^8$. The distribution of protected residues shows that among seven β-strands constituting β2-m, β-strands B and F, connected by the disulfide bond, are most highly protected. Then, β-strands A, C, E, and G adjacent to the disulfide bonded β-strands are also protected. β-Strand D connecting the two β-sheet layers was least protected. The protected residues of β-strands located at the edge of the β-sheet; that is, β-strands A, C, and G, were alternative, and are consistent with the hydrogen bond patterns observed by X-ray analysis (Bjorkman et al. 1987; Katou et al. 2002; Trinh et al. 2002).

In the presence of $Cu^{2+}$, the exchange rates increased by two- to threefold for residues Val24, Tyr26, Glu36, Asp38, Leu40, Lys41, Ala79, Val82, and Val93 (Figs. 5D and 7, and Supplemental Material: Table 1). Although the magnitude was not large, the promotion of exchange by $Cu^{2+}$ was solid for these residues. Most of these affected residues are located in the highly protected β-strands B, C, and F. For residues Phe22, Ser28, Glu44, Leu64, Leu65, Tyr67, Thr68, Leu87, and Lys91, $k_{app}$ was not significantly changed by $Cu^{2+}$ binding. As reflected in the change of protection factors, at physiological pH and at 25°C, $Cu^{2+}$ increased the H/D exchange rate of most of the core residues (Figs. 4C, 5D). Thus, measured by H/D exchange, the effects of $Cu^{2+}$ binding were transmitted to the core of β2-m.

The apparent decay of H signals could also be explained by the molecular association, as it was reported that fibril formation is enhanced in the presence of $Cu^{2+}$ and low concentration of urea (Morgan et al. 2001). However, this is unlikely under our conditions, judging from the constant line shape of aliphatic signals in the 1D spectra recorded during the time course of H/D exchange reaction.

### *Mass spectrometry*

The observed changes in the protein's dynamics and conformation could be due to protein oxidation caused by $Cu^{2+}$, a well-known issue with this cation (Schoneich and Williams 2002). We examined the oxidation of proteins by ESI-MS using a Q-TOF mass spectrometer fitted with a Z-spray nanoflow electrospray ion source (Micromass), which has a very high resolution to be able to detect the modification of the whole β2-m molecule without fragmentation. The protein samples were incubated under the conditions of 0.5 mM β2-m, 50 mM sodium phosphate buffer at pH 7.0 in the absence or presence of 0.5 mM $CuCl_2$ for 3 days at 25°C. The mass spectra clearly showed a small amount of oxidized species with increase of the mass of 16 in both samples incubated in the absence and presence of $Cu^{2+}$ (data not shown). Although the exact oxidation site is not clear, the C-terminal Met99 is most probable site, considering the fact that β2-m has one Met and four His resi-

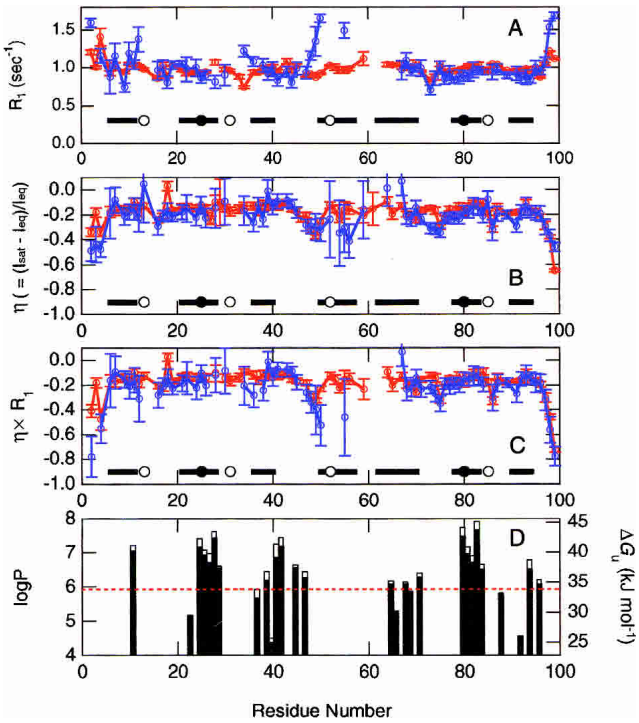


**Figure 5.** The effects of $Cu^{2+}$ binding monitored based on longitudinal relaxation time $R_1$ (*A*), backbone $\{^1H\}$-$^{15}N$ NOE ($\eta = (I_{sat} - I_{eq})/I_{eq}$) (*B*), the product of $R_1$ and NOE ($\eta \times R_1$) (*C*), and amide proton H/D exchange protection factors (*D*), at pH 7.0. Protein and $Cu^{2+}$ concentrations were 0.5 mM. $\{^1H\}$-$^{15}N$ steady-state NOE spectra in the presence (blue) and absence (red) of $Cu^{2+}$ were obtained at 25°C. The locations of seven β-strands (bars), His (empty circles), and Cys (filled circles) residues are indicated. In (*D*), protection factors (*P*) in the presence (filled bars) and absence (empty bars) of $Cu^{2+}$ are shown. The ordinate on the *right* indicates $\Delta G_U$ estimated assuming the EX2 mechanism. The red dotted line indicates the overall $\Delta G_U$ value estimated from Gdn-HCl denaturation at 10°C (Ohhashi et al. 2002).

dues. However, these modified species were independent of $Cu^{2+}$, demonstrating that the observed conformational changes are not due to protein oxidation, but the direct effects caused by binding of $Cu^{2+}$ to His residues.

## Discussion

### *Copper-induced destabilization of* β2-m

The results presented here reveal at the amino acid residue level the conformational and dynamic changes that are produced by the interaction of β2-m with $Cu^{2+}$. Although the binding of metal ions with proteins would generally tend to lower the free energy in the native state, thus stabilizing the native form (Werner et al. 2000), the binding of $Cu^{2+}$ to His residues induces a slightly modified native state of β2-m with increased flexibility and decreased stability (Fig. 1). This conformational change, coupled with the binding of $Cu^{2+}$, can be described in an alternative way that the preferential binding of $Cu^{2+}$ to the destabilized native state shifts the equilibrium between protein substates toward the destabilized state, as represented by the Wyman linkage function (Wyman Jr. 1964). Similar but more drastic conformational change coupled with ligand binding has been reported recently for the binding of Congo red to an amyloidogenic immunoglobulin light chain, SMA, where Congo red binding populates partially unfolded states to enhance aggregation and amyloid fibril formation (Kim et al. 2003).

Heteronuclear NMR enabled the residue-based analysis of $Cu^{2+}$ binding. First, we showed that three histidine residues—that is, His13, His31, and His51—are capable of binding $Cu^{2+}$ at pH 7.0 and two—that is, His13 and His31—at pH 6.5 (Fig. 3). The difference in the binding sites at pH 6.5 and pH 7.0 can be explained by the change in the protonation state of His51 between the two pHs. Because the deprotonation of the His side chain occurs at neutral pH, a slight shift in the pH value will result in a large change in

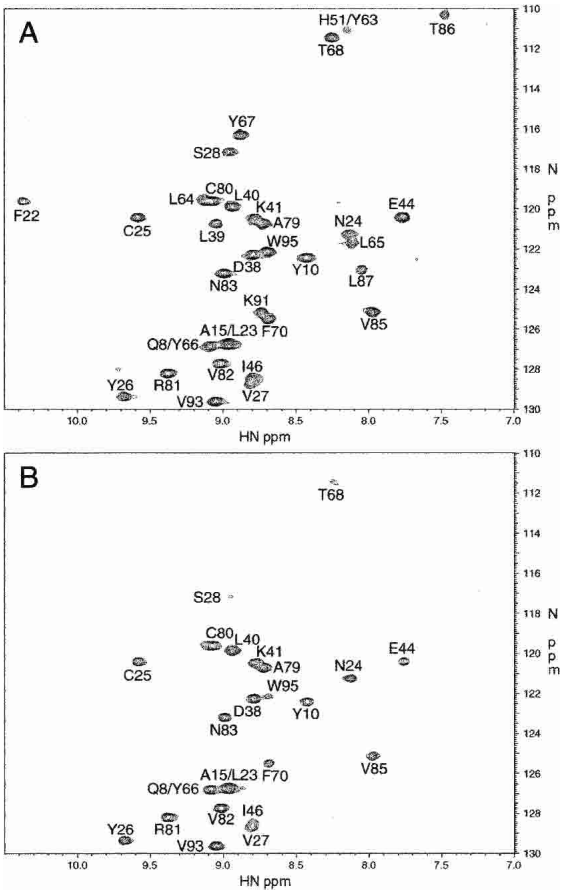


**Figure 6.** H/D exchange of the backbone amide protons of β2-m in the absence of $Cu^{2+}$ at 25°C. Protein concentrations was 0.5 mM. Spectra (*A*) was obtained 40 min after dissolving the protein in $D_2O$ in deuterated phosphate buffer at $pD_r$ 7.0. Only 35 core residues remained after 40 min of exchange. Spectrum (*B*) was obtained after 22 h.

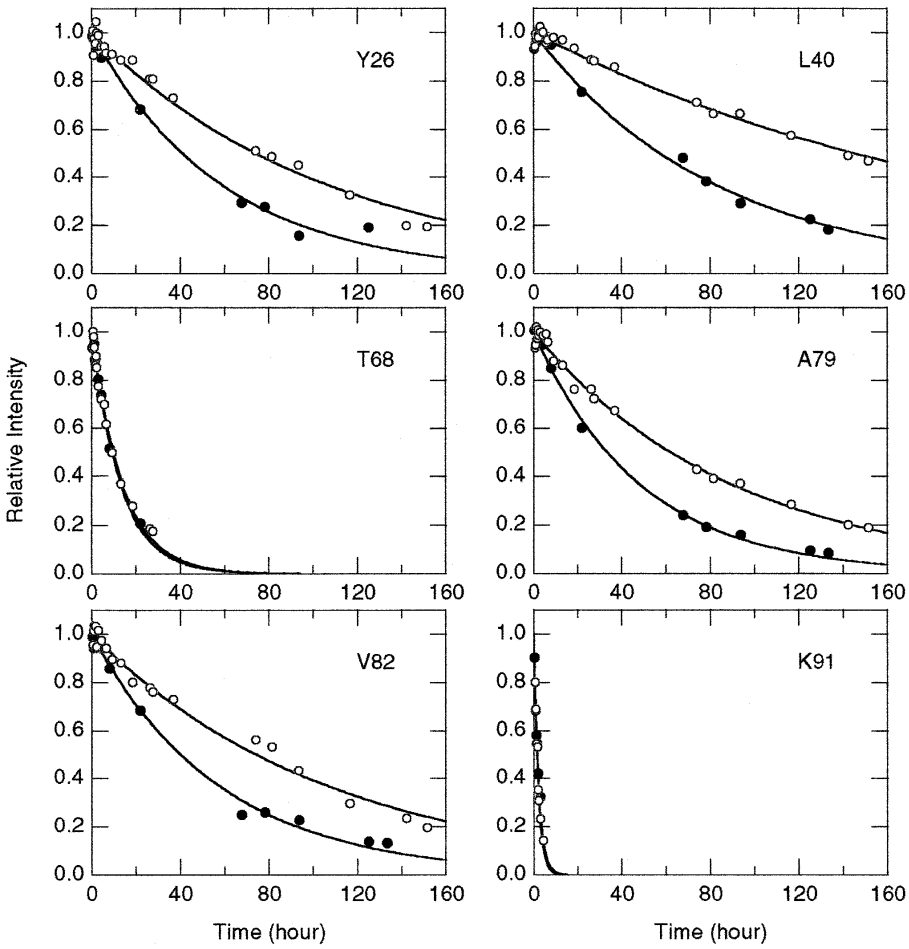


**Figure 7.** Representative examples of peak intensity decay during H/D exchange in the absence (empty circles) and presence (filled circles) of $Cu^{2+}$. The decay kinetics were fitted to a single exponential curve to obtain the backbone proton exchange rate constant ($k_{EX}$).

binding behavior. A link between the deprotonation of histidines and $Cu^{2+}$ binding was also proposed for the Alzheimer β-amyloid and the prion protein (Atwood et al. 1998; Stockel et al. 1998).

Among the three His residues (His13, His31, and His51) responsible for the $Cu^{2+}$ binding at pH 7.0, only the residues near to His51 (i.e., Asp49 and Ser55) revealed the clear increase of backbone dynamics (Fig. 5). Although scarce data points makes solid interpretation difficult, the results suggest that the $Cu^{2+}$ binding at His51 increased pico- to nanosecond time scale backbone dynamics of β-strand D. His51 is located at the middle of β-strand D, whereas others are in the loop or at the end of β-strand. This might be related to the fact that the increase of backbone dynamics is observed for the residues near to His51.

Trinh et al. (2002) reported the crystal structure of a monomeric β2-m that reveals remarkable structural changes in β-strand D relative to the MHC-bound β2-m. Although β-strand D in the MHC-bound form is separated by a β-bulge, the β-bulge is lost in the crystal structure of monomeric β2-m, so that the intermolecular hydrogen bonds are formed with adjacent molecules within the lattice. The conformational change of β-strand D is accompanied by a 180° rotation of His51. They proposed that this drastic structural change observed in β-strand D is a key event leading to amyloid fibril formation. Although such drastic change was not evident in the solution structure studied by NMR (Katou et al. 2002; Verdone et al. 2002), β-strand D is the most unstable strand, as shown by the absence of protected amide protons (Fig. 5D). In other words, it is likely that the backbone dynamics of β-strand D is easily affected by the ligand binding to His51. Thus, the binding of His51 with $Cu^{2+}$ may perturb β-strand D, consequently destabilizing these regions by breaking H-bonds between strands D and E. Increase of backbone dynamics upon ligand binding was also reported for mouse major urinary protein with a hydrophobic pheromone 2-*sec*-butyl-4,5-dihydrothiazole (Zídek et al. 1999).

A possible mechanism of $Cu^{2+}$-induced destabilization of β2-m can be summarized by Figure 4. $Cu^{2+}$ binds to three histidines (His13, His31, and His51) of the native conformation of β2-m at pH 7.0, as monitored by the decrease in peak intensity (Fig. 4A). The product of $R_1$ and NOE values, which is independent of the paramagnetic contributions of $Cu^{2+}$, reflects exclusively the dynamical motion (Fig. 5C; see below). Thus, we suggest that, as monitored by $^1H$-$^{15}N$ NOE, $Cu^{2+}$ binding to His51 increases the pico- to nanosecond time scale backbone dynamics of the residues on β-strand D (Fig. 4B). These local and rapid fluctuations are linked to the increase of the global and slow fluctuations of β2-m core residues, as monitored by H/D exchange (Fig. 4C). In other words, the specific effects on the residues close to the $Cu^{2+}$ binding sites, in particular at His51, may be cooperatively propagated as these residues increase mobility in the adjacent regions by weakening the hydrogen bonds along the backbone and by subtly altering hydrophobic interactions. In addition, the increased dynamics at the N-terminal residues (Fig. 5C) suggests a mobility increase of β-strand A. It is intriguing to consider that the mobility increase of β-strand A reflects the unpairing of strand A, leading to the amyloidogenic partially unfolded intermediates as suggested by Verdone et al. (2002).

On the other hand, Eakin et al. (2002) reported that an increased affinity of $Cu^{2+}$ to the nonnative states compared to the native state gives rise to the overall destabilization. The present results strongly suggest that the $Cu^{2+}$ binding to the native state contributes to destabilizing β2-m, even if the binding to the nonnative state might also be involved.

*Paramagnetic effects*

Although the decrease of the magnitude of NOE suggested the increase in pico- to nanosecond time scale backbone dynamics on βD strand on which His51 exists (Fig. 5B), an alternative possibility of the paramagnetic effects of the $Cu^{2+}$ ions on NOE should be considered carefully. It has long been known that the magnetic interaction between an electronic spin and a nuclear spin causes nuclear relaxation. This so-called paramagnetic effect, can cause drastic increases in both the longitudinal and traverse relaxation rates, resulting in line-broadening and loss of NMR signal, as clearly observed in the $Cu^{2+}$ titration experiment (Fig. 3) and the $R_1$ measurement (Fig. 5A). Here, let us consider the paramagnetic effect on the heteronuclear NOE.

The heteronuclear NOE between amide H-N pair is given by

$$\eta = \frac{I_{sat} - I_{eq}}{I_{eq}} = \frac{\gamma_H R_{Hz\leftrightarrow Nz}}{\gamma_N R_{Nz}} \quad (1)$$

in which $I_{sat}$ and $I_{eq}$ are the peak intensities when $^1H$ is saturated and at thermal equilibrium, respectively, $\gamma_H$ and $\gamma_N$ are the gyromagnetic ratios for $^1H$ and $^{15}N$, respectively, $R_{Nz}$ is the $^{15}N$ longitudinal relaxation rate, and $R_{Hz\leftrightarrow Nz}$ is the cross-relaxation rate. In the presence of paramagnetic metals, $^{15}N$ longitudinal relaxation rate is given by the sum of diamagnetic ($R_{Nz}^{dm}$) and paramagnetic ($R_{Nz}^{pm}$) contributions (Caffrey et al. 1995):

$$R_{Nz} = R_{Nz}^{dm} + R_{Nz}^{pm} \quad (2)$$

The diamagnetic terms consist of dipole–dipole coupling and chemical shift anisotropy components, and described by

$$R_{Hz\leftrightarrow Nz} = \frac{1}{4} d_{NH}^2 [6J(\omega_H + \omega_N) - J(\omega_H - \omega_N)] \quad (3)$$

$$R_{Nz}^{dm} = \frac{1}{4}\left(\hbar \frac{\mu_0}{4\pi}\frac{\gamma_H\gamma_N}{r_{NH}^3}\right)[J(\omega_H - \omega_N) + 3J(\omega_N) + 6J(\omega_H + \omega_N)] + \frac{\omega_N^2 \Delta\sigma^2}{3} J(\omega_N) \quad (4)$$

where $\hbar$ is Plank's constant divided by $2\pi$, $\mu_0$ is the permeability of free space, $\gamma_H$ and $\gamma_N$ are the gyromagnetic ratios of $^1H$ and $^{15}N$, $\omega_H$ and $\omega_N$ are the Larmor frequencies of $^1H$ and $^{15}N$, $r_{NH}$ is the N—H bond length, and $\Delta\sigma$ is the chemical shift anisotropy value. $J(\omega)$ is the spectral density function, defined as

$$J(\omega) = \frac{2\tau_c}{5(1 + (\omega\tau_c)^2} \quad (5)$$

where $\tau_c$ is the correlation time.

The paramagnetic contribution to the longitudinal relaxation rate is essentially dominated by the dipole–dipole coupling between the electron spin and the nuclear spin, and is expressed by

$$R_{Nz}^{pm} = \frac{2}{15} S(S+1)\left(\hbar \frac{\mu_0}{4\pi}\frac{\gamma_N\gamma_S}{r_{NS}^3}\right)[J(\omega_N\text{-}\omega_S) + 3J(\omega_N) + 6J(\omega_N + \omega_S)] \approx \frac{2}{15} S(S+1)\left(\hbar \frac{\mu_0}{4\pi}\frac{\gamma_N\gamma_S}{r_{NS}^3}\right)[3J(\omega_N) + 7J(\omega_S)] \quad (6)$$

$$J(\omega) = \frac{2\tau_S}{5(1 + (\omega\tau_s)^2)} \quad (7)$$

where $S$ is the electron spin quantum number, $\gamma_S$ is the gyromagnetic ratio for the electron, $r_{NS}$ is the nuclear-electron distance, $\omega_S$ is the Larmor frequency of electron spin, and $\tau_S$ is the correlation time of the electron. The second equality in equation 6 was obtained because $\omega_S >> \omega_N$.

By substituting equations 2–7 into equation 1, the heteronuclear NOE could be simulated as a function of rotational correlation time, τ, at different nuclear-electron distances (Fig. 8A). In the absence of paramagnetic effect ($r_{NS} \geq 15$Å), the heteronuclear NOE exhibits the strong dependence on the rotational correlation time, ranging from a minimum of approximately −4 at the correlation time less than 0.1 nsec to a maximum approximately −0.14 at the correlation time larger than 10 nsec. In the presence of paramagnetic effect, this pronounced NOE at longer correlation time strongly reduced (approaches to zero), depending on the nuclear–electron distance. The rotational correlation time of β2-m (11.7 kD) is estimated to be 5.5 nsec using the Stokes-Einstein equation. In this region, the NOE is originally close to 0, and the paramagnetic effect is relatively weak. Most importantly, the paramagnetic effect is always positive, increasing the NOE (i.e., bringing the NOE close to 0).

In the present results, we observed synchronous increase in $R_1$ and decrease in NOE around three histidine residues upon addition of $Cu^{2+}$ (Fig. 5A,B). Although the increase in $R_1$ could be explained by the paramagnetic contribution as expressed in equation 2, the decrease in NOE could not be explained by the simple binding of $Cu^{2+}$ ion to these residues, because the paramagnetic effect always increases the NOE value. To account for this, the intramolecular motion should be incorporated as provided by Lipari-Szabo model free formalism (Lipari and Szabo 1982a,b). Then, the spectral density function is given by

$$J(\omega) = \frac{2}{5}\left[\frac{S^2\tau_m}{(1+(\omega\tau_m)^2)} + \frac{(1+S^2)\tau}{(1+(\omega\tau)^2)}\right] \quad (8)$$

where $\tau^{-1} = \tau_m^{-1} + \tau_e^{-1}$, $S^2$ is the square of the generalized order parameter, $\tau_m$ is the overall rotational correlation time,

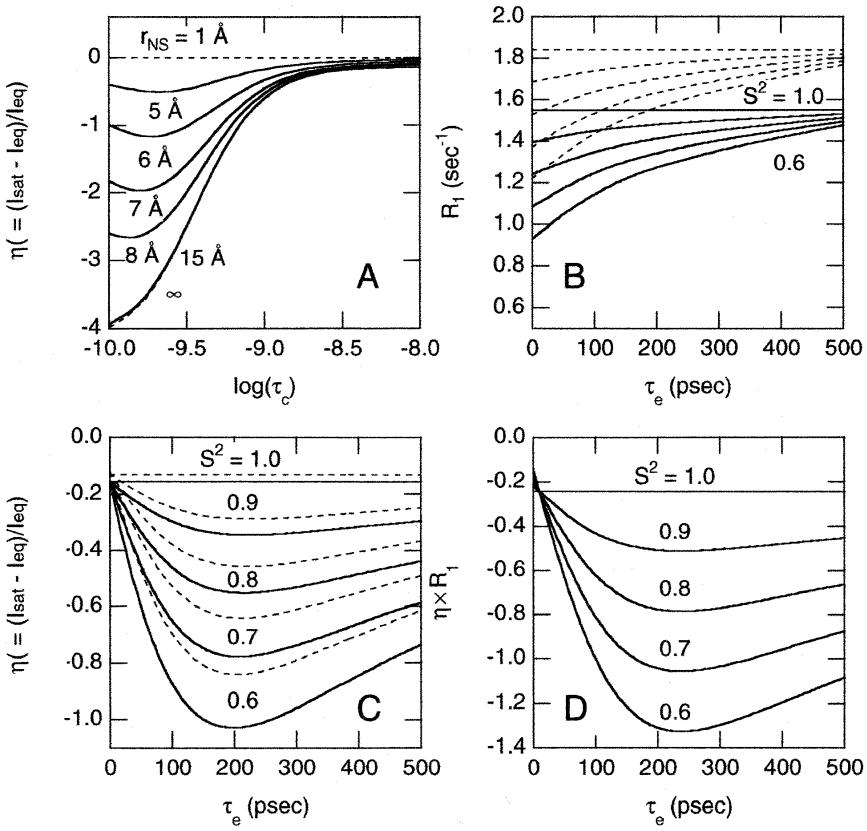


**Figure 8.** (*A*) $^1$H-$^{15}$N heteronuclear NOE simulated as a function of correlation time with different $^{15}$N-electron distance ($r_{NS}$). Dashed lines show two extreme conditions ($r_{NS}$ = 1 Å or ∞). (*B–D*) The effect of intramolecular motions and paramagnetic contribution. The values of $R_1$ (*B*), NOE (*C*), and the product of $R_1$ and NOE (*D*) was plotted as a function of the effective correlation time for internal motions with different generalized order parameter values. In (*B*), the values of $S^2$ are 1.0, 0.9, 0.8, 0.7, and 0.6 from the *top*. The solid lines are obtained in the absence of $Cu^{2+}$, while the dotted lines are in the presence of paramagnetic effect ($r_{NS}$ = 8 Å and $\tau_c$ = 5.5 nsec). Note that in (*D*), both lines are overlapped. The values used for simulation were $\hbar = 1.05 \times 10^{-34}$ J·s, $\mu_0 = 4\pi \times 10^{-7}$ T$^2$·J$^{-1}$·m$^3$, $\gamma_H = 2.6752 \times 10^8$ T$^{-1}$·sec$^{-1}$, $\gamma_N = -2.712 \times 10^7$ T$^{-1}$·sec$^{-1}$, $\omega_H$ = 800.33 MHz, $\omega_N$ = 81.13 MHz, $r_{NH}$ = 1.02 Å, $\Delta\sigma$ = −160 ppm, S = 3/2, $\gamma_S = -1.76 \times 10^{11}$ T$^{-1}$·sec$^{-1}$, $\omega_S$ = 526.5 GHz, and $\tau_S$ = 0.05 nsec.

and $\tau_e$ is the effective correlation time for internal motions. By using equation 8 instead of equation 5, the $R_1$ and NOE are simulated as a function of effective correlation time (Fig. 8B,C). With this formula, it is clear that the NOE is highly dependent on both the $S^2$ (amplitude of the internal motions) and $\tau_e$ (correlation time of the internal motions). Those simulations also show clearly that both $R_1$ and NOE are always increased if a paramagnetic contribution is present. Conversely, the product of $R_1$ and NOE does not involve the paramagnetic contribution, as predicted from equations 1–3. Indeed, the simulated value of the product of $R_1$ and NOE does not depend on the presence of a paramagnetic effect, but rather exclusively depends on the internal dynamic motions (Fig. 8D). Although the quantitative determination of the $S^2$ and $\tau_e$ needs comprehensive measurements of the other relaxation parameters, that is, $R_1$ and $R_2$ at various magnetic field strengths, the significant decrease in the NOE strongly suggests the $Cu^{2+}$-induced increase of the mobility in the pico- to nanosecond time scale.

### *Protected core of* β2-m

H/D exchange clarified the protected core of β2-m. Protection factors obtained from the H/D exchange experiment can be related to the parameters of protein unfolding at each amide site assuming a two-process model between the folded ($N$) and unfolded ($U$) states and the exchanged state ($X$):

$$\mathrm{N} \underset{k_\mathrm{R}}{\overset{k_\mathrm{u}}{\rightleftarrows}} \mathrm{U} \overset{k_\mathrm{EX}}{\rightarrow} \mathrm{X} \qquad \text{(Scheme 1)}$$

where $k_U$ and $k_R$ represent the unfolding and refolding rate constants, respectively, and $k_{EX}$ is the intrinsic exchange rate (Kim et al. 1993; Englander 2000). The equilibrium constant ($K_U$) between $N$ and $U$ is related to the microscopic rate constants by $K_U = k_U/k_R$. Under conditions where the conformational equilibrium is much faster than the intrinsic rate of exchange (EX2 limit), the apparent exchange rate is represented by $K_U k_{EX}$. Here, the protection factor ($P$) corresponds to $1/K_U$ and $\Delta G_U$ is estimated by $\Delta G_U = RT \ln P$. Under the other extreme condition where $k_{EX}$ is much faster than the refolding rate constant $k_R$, the apparent rate constant represents $k_U$ (EX1 limit). Under intermediate conditions where $k_R$ is comparable to $k_{EX}$, $\Delta G_U$ estimated on the basis of EX2 limit would be larger than the true value.

We converted the protection factors into $\Delta G_U$ assuming the EX2 limit (Fig. 5D, right ordinate). The $\Delta G_U$ values for the highly protected residues are 30–45 kJ/mole. It is generally considered that, while the largest $\Delta G_U$ values obtained from the amide H/D exchange experiment represent those of global unfolding, the local fluctuation or penetration of water molecules into the protein interior decreases the $\Delta G_U$ value, thus causing the wide distribution of observed $\Delta G_U$ (Kim et al. 1993; Englander 2000). In this context, the $\Delta G_U$ value for global unfolding of β2-m at 25°C extrapolated from the thermal denaturation is 23 kJ/mole and $\Delta G_U$ at 10°C obtained from the Gdn-HCl denaturation is 34 kJ/mole (Ohhashi et al. 2002). The $\Delta G_U$ values for the highly protected amide protons are larger than those for global unfolding. However, the exact comparison of these values is difficult because of the probable deviation from a two-state mechanism, in particular in the presence of $Cu^{2+}$. Although further study is necessary, it is likely that the mechanism of H/D exchange also deviates from the EX2 mechanism. Alternatively, the denatured form of β2-m under physiological conditions retains the native-like core made of β-strands B, C, and F, which prevents rapid H/D exchange. The maximal decrease in $\Delta G_U$ upon $Cu^{2+}$ binding estimated from the H/D exchange experiment is about 2 kJ/mole, less than that obtained for the thermal denaturation (10 kJ/mole). This is partly explained by the fact that, under the present conditions of H/D exchange at $pD_r$ 7.0, not all of the three histidine residues were fully complexed with $Cu^{2+}$. Moreover, the difference suggests the contribution of the $Cu^{2+}$ binding to the denatured state as indicated by Eakin et al. (2002).

In conclusion, in light of its role in the amyloid fibril formation of β2-m in long-term hemodialysis, $Cu^{2+}$ would act by making the thermodynamics and the kinetics more favorable for the formation of the amyloidogenic β2-m intermediate needed for fibril formation. $Cu^{2+}$ binding are likely to increase the local and rapid fluctuations of the binding site at His51 as observed by $\{^1H\}$-$^{15}N$ NOE measurement, which are then propagated to the core of the molecule, leading to the global and slow fluctuations of the entire molecule as indicated by H/D exchange. This contributes to the $Cu^{2+}$-induced overall destabilization of the β2-m molecule, probably increasing the equilibrium population of amyloidogenic intermediate. The increased flexibility of β-strand A may expose the minimal amyloidogenic region found in β-strands B and C, identified by Khozukh et al. (2002), which may trigger fibril formation, as suggested by Verdone et al. (2002). Additional binding of $Cu^{2+}$ ions to the denatured state and preformed amyloid fibrils, not examined here, would further promote the fibril formation. Detailed characterization of the amyloid fibril formation in the presence of $Cu^{2+}$ ions will be important to clarify the connection between a destabilization effect of $Cu^{2+}$ ions and amyloid fibril formation.

## Materials and methods

### *Recombinant* β2-m

Recombinant human β2-m with four additional residues at the N terminus (Glu(-4)-Ala(-3)-Tyr(-2)-Val(-1)-Ile(1)) was expressed

in methylotrophic yeast *Picihia pastoris* and purified as described previously (Kozhukh et al. 2002; Ohhashi et al. 2002). It has been confirmed that recombinant β2-m is indistinguishable from β2-m derived from patients with respect to amyloid fibril formation. Uniformly $^{15}$N-labeled β2-m was obtained using $^{15}$N-ammonium hydroxide as the sole nitrogen source.

### *CD measurements*

CD measurements were done with a Jasco spectropolarimeter Model J-720. The results are expressed as mean residue ellipticity. Thermal denaturation was carried out in 10 mM sodium phosphate buffer (pH 6.5 and pH 7.0) containing 300 mM KCl. The protein and $CuCl_2$ concentrations were 5 μM and 50 μM, respectively. Heating was performed at 0.5°C/min up to 85°C. Thermal denaturation was reversible in both the presence and absence of $CuCl_2$ judging from the signal intensity obtained after decreasing the temperature. It is noted that, in the presence of $CuCl_2$ at pH 6.5, a high concentration of salt (i.e., 300 mM KCl) was necessary to prevent the aggregation at high temperature. The transitions in the absence of $CuCl_2$ at 300 mM KCl were the same as those at 100 mM KCl at both pH 6.5 and pH 7.0. The unfolding curves were analyzed on the basis of a two-state transition between the native state ($N$) and the unfolded state ($U$): $N \rightleftharpoons U$, with the standard thermodynamic equations (Nishii et al. 1995). The observed unfolding curves were fitted to the theoretical curve to obtain the following thermodynamic parameters: the midpoint temperature of unfolding ($T_m$), the enthalpy change at $T_m$ ($\Delta H_m$), and the free energy change of unfolding at 25°C ($\Delta G_U$ [25°C]). It is noted that a constant value (5.6 kJ/mole/K) was assumed for the heat capacity change of unfolding ($\Delta C_{p,U}$), which was obtained based on the pH-dependence of the unfolding transition curves monitored by CD (J. Kardos and Y. Goto, unpubl.).

### *NMR measurements*

The spectra were recorded mainly on a 500 MHz spectrometer (Bruker DRX 500) as described before (Katou et al. 2002). For the relaxation measurements ($R_1$ and NOE), a 800 MHz spectrometer (Bruker DRX 800) was used. Processing of the data acquired was done using nmrDraw and PIPP (Garrett et al. 1991; Delaglio et al. 1995). For the titration experiments, a $^{15}$N-labeled sample (0.47 mM) was titrated with $CuCl_2$ and the $^1$H-$^{15}$N HSQC spectra were measured at 25°C. The buffer used was 50 mM sodium phosphate containing 100 mM KCl at pH 7.0 or pH 6.5.

The measurement of steady-state heteronuclear {$^1$H}-$^{15}$N NOE was carried out at 25°C according to the procedure described by Farrow et al. (1994). The NOE values were calculated as the ratios of peak heights from spectra obtained with and without a $^1$H saturation period. The protein and $CuCl_2$ concentrations were 0.5 mM, in 50 mM sodium phosphate buffer (pH 7.0). It is noted that because NMR spectra were measured at high protein concentrations in comparison with those used for CD measurements, a low molar ratio of $Cu^{2+}$ over protein concentration is enough to obtain the stoichiometric binding.

The measurement of $R_1$ was carried out as described by Farrow et al. (1994) at 25°C with relaxation times of 20, 100, 200, 300, 400, 600, 800, and 1000 msec. The peak intensity as a function of relaxation time was analyzed on the basis of a single exponential decay. The same protein solutions as used for NOE measurements were used.

H/D exchange in the presence and absence of $Cu^{2+}$ was performed at 25°C and $pD_r$ 7.0, where $pD_r$ is the pH meter reading without correction for the isotope effect. Both the protein and the $CuCl_2$ concentrations were 0.5 mM. The amide proton decay was followed by measuring peak intensities in the $^1$H-$^{15}$N HSQC spectra. The decay curves were fitted to a single exponential curve to obtain the apparent rate constant of exchange ($k_{app}$).

## Electronic supplemental material

Supplemental material is presented for H/$^2$H exchange protection factors of β2-microglobulin in the absence and presence of $CuCl_2$ (Table 1).

## Acknowledgments

We thank Dr. Gennady Khozhuk for the preparation of the $^{15}$N-labeled β2-m, Dr. Yoshinori Satomi and Professor Takafumi Takao for mass spectroscopy, and Professor Takahisa Ikegami for helpful suggestions. This work was supported in part by Grants-in-Aid for Scientific Research from the Japanese Ministry of Education, Science, Sports and Culture. J.K. is supported by Japan Society for the Promotion of Science, and J.V. was supported by the COE Foreign Fellowship Grant from the Osaka University.

The publication costs of this article were defrayed in part by payment of page charges. This article must therefore be hereby marked "advertisement" in accordance with 18 USC section 1734 solely to indicate this fact.

## References

Alexandrescu, A. 2001. An NMR-based quenched hydrogen exchange investigation of model amyloid fibrils formed by cold shock protein A. *Pac. Symp. Biocomput.* 67–78.

Atwood, C.S., Moirs, R.D., Huang, X., Scarpa, R.C., Bacarra, N.M., Romano, D.M., Hartshorn, M.A., Tanzi, R.E., and Bush, A.L. 1998. Dramatic aggregation of Alzheimer Aβ by $Cu^{2+}$ is induced by conditions representing physiological acidosis. *J. Biol. Chem.* **273:** 12817–12826.

Bai, Y., Milne, J.S., Mayne, L., and Englander, S.W. 1993. Primary structure effects on peptide group hydrogen exchange. *Proteins* **17:** 75–86.

Bjorkman, P.J., Saper, M.A., Samraoui, B., Bennett, W.S., Strominger, J.L., and Wiley, D.C. 1987. Structure of the human class I histocompatibility antigen, HLA-A2. *Nature* **329:** 506–512.

Caffrey, M., Simorre, J.-P., Cusanovich, M., and Marion, D. 1995. Characterization of the dynamic properties of *Rhodobacter capsulatus* ferricytochrome *c′*—A 28 kDa paramagnetic heme protein. *FEBS Lett.* **368:** 519–522.

Chiti, F., De Lorenzi, E., Grossi, S., Mangione, P., Giorgetti, S., Caccialanza, G., Dobson, C.M., Merlini, G., Ramponi, G., and Bellotti, V. 2001a. A partially structured species of $\beta_2$-microglobulin is significantly populated under physiological conditions and involved in fibrillogenesis. *J. Biol. Chem.* **276:** 46714–46721.

Chiti, F., Mangione, P., Andreola, A., Giorgetti, S., Stefani, M., Dobson, C.M., Bellotti, V., and Taddei, N. 2001b. Detection of two partially structured species in the folding process of the amyloidogenic protein $\beta_2$-microglobulin. *J. Mol. Biol.* **307:** 379–391.

Connelly, G.P., Bai, Y., Jeng, M.-F., and Englander, S.W. 1993. Isotope effects in peptide group hydrogen exchange. *Proteins* **17:** 87–92.

Davis, D.P., Gallo, G., Vogen, S.M., Dul, J.L., Sciaretta, K.L., Kumar, A., Raffen, R., Stevens, F.J., and Argon, Y. 2001. Both the environment and somatic mutations govern the aggregation pathway of pathogenic immunoglobulin light chain. *J. Mol. Biol.* **313:** 1021–1034.

Delaglio, F., Grzesiek, S., Vuister, G., Zhu, G., Pfeifer, J., and Bax, A. 1995. NMRPipe: A multidimensional spectral processing system based on UNIX Pipes. *J. Biomol. NMR* **6:** 277–293

Eakin, C.M., Knight, J.D., Morgan, C.J., Gelfand, M.A., and Miranker, A.D. 2002. Formation of a copper specific binding site in non-native states of β-2-microglobulin. *Biochemistry* **41:** 10646–10656.

Englander, S.W. 2000. Protein folding intermediates and pathways studied by hydrogen exchange. *Annu. Rev. Biophys. Biomol. Struct.* **29:** 213–238.

Esposito, G., Michelutti, R., Verdone, G., Viglino, P., Hernandez, H., Robinson, C.V., Amoresano, A., Dal Piaz, F., Monti, M., Pucci, P., et al. 2000. Removal of the N-terminal hexapeptide from human $\beta_2$-microglobulin facilitates protein aggregation and fibril formation. *Protein Sci.* **9:** 831–845.

Farrow, N.A., Muhandiram, R., Singer, A.U., Pascal, S.M., Kay, C.M., Gish, G., Shoelson, S.E., Pawson, T., Forman-Kay, J.D., and Kay, L.E. 1994. Backbone dynamics of a free and phosphopeptide-complexed src homology 2 domain studied by $^{15}$N NMR relaxation. *Biochemistry* **33:** 5984–6003.

Garrett, D.S., Powers, R., Gronenborn, A.M., and Clore, G.M. 1991. A common sense approach to peak picking in two, three and four dimensional spectra using automatic computer analysis of contour diagrams. *J. Magn. Reson.* **95:** 214–220.

Geyjo, F. and Arakawa, M. 1990. Dialysis amyloidosis: Current disease concepts and new perspectives for its treatment. *Contrib. Nephrol.* **78:** 47–60.

Gejyo, F., Yamada, T., Odani, S., Nakagawa, Y., Arakawa, M., Kunimoto, T., Kataoka, H., Suzuki, M., Hirasawa, Y., Shirahama, T., et al. 1985. A new form of amyloid protein associated with chronic hemodialysis was identified as $\beta_2$-microglobulin. *Biochem. Biophys. Res. Commun.* **129:** 701–706.

Hasegawa, K., Ohhashi, Y., Yamaguchi, I., Takahashi, N., Tsutsumi, S., Goto, Y., Gejyo, F., and Naiki, H. 2003. Amyloidogenic synthetic peptides of β2-microglobulin—A role of the disulfide bond. *Biochem. Biophys. Res. Commun.* **304:** 101–106.

Heegaard, N.H., Sen, J.W., Kaarsholm, N.C., and Nissen, M.H. 2001. Conformational intermediate of the amyloidogenic protein $\beta_2$-microglobulin at neutral pH. *J. Biol. Chem.* **276:** 32657–32662.

Hoshino, M., Hagihara, Y., Nishii, I., Yamazaki, T., Kato, H., and Goto, Y. 2000. High mobility of the phospholipid binding loop of human $\beta_2$-glycoprotein I domain V revealed by heteronuclear NMR. *J. Mol. Biol.* **304:** 927–940.

Hoshino, M., Katou, H., Hagihara, Y., Hasegawa, K., Naiki, H., and Goto, Y. 2002. Mapping the core of the $\beta_2$-microglobulin amyloid fibrils by H/D exchange. *Nat. Struct. Biol.* **9:** 332–336.

Ippel, J.H., Olofsson, A., Schleucher, J., Lundgren, E., and Wijmenga, S.S. 2002. Probing solvent accessibility of amyloid fibrils by solution NMR spectroscopy. *Proc. Natl. Acad. Sci.* **99:** 8648–8653.

Jones, S., Manning, J., Kad, N.M., and Radford, S.E. 2003, Amyloid-forming peptides from β2-microglobulin—Insights into the mechanism of fibril formation *in vitro*. *J. Mol. Biol.* **325:** 249–257.

Kad, N.M., Thomson, N.H., Smith, D.P., Smith, D.A., and Radford, S.E. 2001. $\beta_2$-Microglobulin and its deamidated variant, N17D form amyloid fibrils with a range of morphologies *in vitro*. *J. Mol. Biol.* **313:** 559–571.

Kad, N.M., Myers, S.L., Smith, D.P., Smith, D.A., Radford, S.E., and Thomson, N.H. 2003. Hierarchical assembly of β2-microglobulin amyloid *in vitro* revealed by atomic force microscopy. *J. Mol. Biol.* **330:** 785–797.

Katou, H., Kanno, T., Hoshino, M., Hagihara, Y., Tanaka, H., Kawai, T., Hasegawa, K., Naiki, H., and Goto, Y. 2002. The role of disulfide bond in the amyloidogenic state of $\beta_2$-microglobulin studied by heteronuclear NMR. *Protein Sci.* **11:** 2218–2229.

Kelly, J.W. 1998. The alternative conformations of amyloidogenic proteins and their multi-step assembly pathways. *Curr. Opin. Struct. Biol.* **8:** 101–106.

Kim, K.S., Fuchs, J.A., and Woodward, C.K. 1993. Hydrogen exchange identifies native state motional domains important in protein folding. *Biochemistry* **32:** 9600–9608.

Kim, Y.-S., Randolph, T.W., Manning, M.C., Stevens, F.J., and Carpenter, J.F. 2003. Congo red populates partially unfolded states of an amyloidogenic protein to enhance aggregation and amyloid fibril formation. *J. Biol. Chem.* **278:** 10842–10850.

Koradi, R., Billeter, M., and Wüthrich, K. 1996. MOLMOL: A program for display and analysis of macromolecular structures. *J. Mol. Graph.* **14:** 51–55.

Kozhukh, G., Hagihara, Y., Kawakami, T., Hasegawa, K., Naiki, H., and Goto, Y. 2002. Investigation of the peptide responsible for amyloid fibril formation of $\beta_2$-microglobulin by *Achromobacter* protease I. *J. Biol. Chem.* **277:** 1310–1315.

Kramer, M.L., Kratzin, H.D., Schmidt, B., Romer, A., Windl, O., Liemann, S., Hornemann, S., and Kretzchmar, H. 2001. Prion protein binds copper within the physiological concentration range. *J. Biol. Chem.* **276:** 16711–16719.

Lipari, G. and Szabo, A. 1982a. Model-free approach to the interpretation of nuclear magnetic resonance relaxation in macromolecules. 1. Theory and range of validity. *J. Am. Chem. Soc.* **104:** 4546–4559.

———. 1982b. Model-free approach to the interpretation of nuclear magnetic resonance relaxation in macromolecules. 2. Analysis of experimental results. *J. Am. Chem. Soc.* **104:** 4559–4570.

Liu, S.T., Howlett, G., and Barrow, C.J. 1999. Histidine 13 is a crucial residue in the zinc ion-induced aggregation of the Aβ peptide of Alzheimer's disease. *Biochemistry* **38:** 9373–9378.

López de la Paz, M., Goldie, K., Zurdo, J., Lacroix, E., Dobson, C.M., Hoenger, A., and Serrano, L. 2002. *De novo* designed peptide-based amyloid fibrils. *Proc. Natl. Acad. Sci.* **99:** 16052–16057.

McParland, V.J., Kad, N.M., Kalverda, A.P., Brown, A., Kirwin-Jones, P., Hunter, M.G., Sunde, M., and Radford, S.E. 2000. Partially unfolded states of $\beta_2$-microglobulin and amyloid formation *in vitro*. *Biochemistry* **39:** 8735–8746.

McParland, V.J., Kalverda, A.P., Homans, S.W., and Radford, S.E. 2002. Structural properties of an amyloid precursor of $\beta_2$-microglobulin. *Nat. Struct. Biol.* **9:** 326–331.

Miura, T., Suzuki, K., Kohata, N., and Takeuchi, H. 2000. Metal binding modes of Alzheimer's amyloid β-peptide in insoluble aggregates and soluble complexes. *Biochemsitry* **39:** 7024–7031.

Morgan, C.J., Gelfand, M., Atreya, C., and Miranker A.D. 2001. Kidney dialysis-associated amyloidosis: A molecular role for copper in fiber formation. *J. Mol. Biol.* **309:** 339–345.

Naiki, H., Hashimoto, N., Suzuki, S., Kimura, H., Nakakuki, K., and Gejyo, F. 1997. Establishment of a kinetic model of dialysis-related amyloid fibril extension *in vitro*. *Amyloid* **4:** 223–232.

Nishii, I., Kataoka, M., and Goto, Y. 1995. Thermodynamic stability of the molten globule states of apomyoglobin. *J. Mol. Biol.* **250:** 223–238.

Ohhashi, Y., Hagihara, Y., Khozukh, G., Hoshino, M., Hasegawa, K., Yamaguchi, I., Naiki, H., and Goto, Y. 2002. The intrachain disulfide bond of $\beta_2$-microglobulin is not essential for the immunoglobulin fold at neutral pH but is essential for amyloid fibril formation at acidic pH. *J. Biochem.* **131:** 45–52.

Rochet, J.C. and Lansbury Jr., P.T. 2000. Amyloid fibrillogenesis: Themes and variations. *Curr. Opin. Struct. Biol.* **10:** 60–68.

Schoneich, C. and Williams, T.D. 2002. Cu(II)-catalyzed oxidation of β-amyloid peptide targets His13 and His14 over His6: Detection of 2-Oxo-histidine by HPLC-MS/MS. *Chem. Res. Toxicol.* **15:** 717–722.

Stockel, J., Safar, J., Wallace, A.C., Cohen, F.E., and Prusiner, S.B. 1998. Prion protein selectively binds copper ions. *Biochemistry* **37:** 7185–7193.

Sunde, M., Serpell, L.C., Bartlam, M., Fraser, P.E., Pepys, M.B., and Blake, C.C. 1997. Common core structure of amyloid fibrils by synchrotron X-ray diffraction. *J. Mol. Biol.* **273:** 729–739.

Tollinger, M., Skrynnikov, N.R., Mulder, F.A., Forman-Kay, J.D., and Kay, L.E. 2001. Slow dynamics in folded and unfolded states of an SH3 domain. *J. Am. Chem. Soc.* **123:** 11341–11352.

Trinh, C.H., Smith, D.P., Kalverda, A.P., Phillips, S.E.V., and Radford, S.E. 2002. Crystal structure of monomeric human β2-microglobulin reveals clues to its amyloidogenic properties. *Proc. Natl. Acad. Sci.* **99:** 9771–9776.

Verdone, G., Corazza, A., Viglino, P., Pettirossi, F., Giorgetti, S., Mangione, P., Andreola, A., Stoppini, M., Bellotti, V., and Esposito, G. 2002. The solution structure of human $\beta_2$-microglobulin reveals the prodromes of its amyloid transition. *Protein Sci.* **11:** 487–499.

Viles, J.H., Donne, D., Kroon, G., Prusiner, S.B., Cohen, F.E., Dyson, H.J., and Wright, P.E. 2001. Local structural plasticity of the prion protein. Analysis of NMR relaxation dynamics. *Biochemistry* **40:** 2743–2753.

Werner, J.M., Knott, V., Handford, P.A., Campbell, I.D., and Downing, A.K. 2000. Backbone dynamics of a cbEGF domain pair in the presence of calcium. *J. Mol. Biol.* **296:** 1065–1078.

Wyman Jr., J. 1964. Linked functions and reciprocal effects in hemoglobin: A second look. *Adv. Protein Chem.* **19:** 223–286.

Zídek, L., Novotny, M.V., and Stone, M.J. 1999. Increased protein backbone conformational entropy upon hydrophobic ligand binding. *Nat. Struct. Biol.* **6:** 1118–1121.